SUPPLEMENTARY MATERIAL

SHRIMP U-Pb dating of prograde and retrograde UHT metamorphism as exemplified by Sri Lankan granulites

K. Sajeev[1], I. S. Williams[2] and Y. Osanai[3]

[1]*Centre for Earth Sciences, Indian Institute of Science, Bangalore 560012, India*
[2]*Research School of Earth Sciences, The Australian National University, Canberra ACT 0200, Australia*
[3]*Division of Evolution of Earth Environments, Faculty of Social and Cultural Studies, Kyushu University, 744 Motooka, Fukuoka, 819-0395 Japan*

PETROLOGY

The sample of quartz-bearing granulite from Gompola (3107B) contains porphyroblasts of garnet, orthopyroxene, quartz and sillimanite. The key UHT assemblage sapphirine + quartz occurs as inclusions in the garnet cores. The assemblage orthopyroxene + sillimanite + quartz is present as inclusions within the garnet rims, and also as intergrowths around the boundaries of partly resorbed garnet grains. The sample of quartz-free granulite from Talatuoya (0505E) is dominated by orthopyroxene-sapphirine symplectites with or without fine-grained relics of garnet. Quartz and sillimanite are absent. Biotite is present in all the studied thin sections, but is clearly part of a retrograde assemblage formed during late-stage hydration.

Sajeev and Osanai (2004) recognized four types of mineral assemblage: Type A, quartz and sillimanite present, Type B quartz absent, sillimanite present, Type C quartz and sillimanite absent, and Type D garnet, quartz and sillimanite absent. An outline of the mineral reactions in each assemblage is summarized in Supplementary Table DR1.

Type-A
Qtz-Sil present

Spr-Qtz inclusion in Grt	Spr + Qtz = Grt + Sil
	Grt + Spr + Qtz = Opx (1,2) + Sil
Opx-Sil-Qtz inclusion in Grt	Opx (3) + Sil + Qtz = Crd
Opx-Sil-Qtz intergrowth	Opx (3) + Sil + Qtz = Grt + Crd
Crd moat on Opx-Sil-Qtz	
Opx-Sil intergrowth	-
Spr-Crd symplectite	-
	-
Opx-Crd±Spl symplectite	Grt + Qtz = Opx (5)+ Crd ± Pl
Opx-Spr symplectite	-
Spr-Opx/Opx-Spl symlectite	-
Bt rim or intergrowth	Grt + Kfs + Qtz + V = Bt + Crd
Krn forming reaction	-
Late Opx rim on Bt	Bt + Qtz + Grt = Opx (8)+ Kfs + Crd + V

Peak metamorphism

Type-B
Qtz-absent Sil present

Spr-Qtz inclusion in Grt	-
	-
Opx-Sil-Qtz inclusion in Grt	-
Opx-Sil-Qtz intergrowth	-
Crd moat on Opx-Sil-Qtz	-
Opx-Sil intergrowth	Grt + Crd = Opx (4)+ Sil
Spr-Crd symplectite	-
	-
Opx-Crd±Spl symplectite	Grt = Opx (5) + Crd
Opx-Spr symplectite	-
Spr-Opx/Opx-Spl symlectite	-
Bt rim or intergrowth	Opx (2) + Kfs + L = Bt + Crd
Krn forming reaction	-
Late Opx rim on Bt	-

Peak metamorphism

Type-C
Qtz-Sil absent

Spr-Qtz inclusion in Grt	-
	-
Opx-Sil-Qtz inclusion in Grt	-
Opx-Sil-Qtz intergrowth	-
Crd moat on Opx-Sil-Qtz	-
Opx-Sil intergrowth	-
Spr-Crd symplectite	Opx (2, 4) + Sil = Spr + Crd
	Grt + Sil = Spr + Crd
Opx-Crd±Spl symplectite	Grt = Opx (5) + Crd
Opx-Spr symplectite	Grt = Opx (6) + Spr + Crd
Spr-Opx/Opx-Spl symlectite	Opx (6) + Spr = Opx (7) + Spl
Bt rim or intergrowth	Opx (2) + Kfs + L = Bt + Crd
Krn forming reaction	-
Late Opx rim on Bt	-

Peak metamorphism

Type-D
Qtz-Sil-Grt absent

Spr-Qtz inclusion in Grt	-
	-
Opx-Sil-Qtz inclusion in Grt	-
Opx-Sil-Qtz intergrowth	-
Crd moat on Opx-Sil-Qtz	-
Opx-Sil intergrowth	-
Spr-Crd symplectite	-
	-
Opx-Crd±Spl symplectite	Grt = Opx (5) + Crd
Opx-Spr symplectite	Grt = Opx (6) + Spr + Crd
Spr-Opx/Opx-Spl symlectite	-
Bt rim or intergrowth	Opx (2) + Kfs + L = Bt + Crd
Krn forming reaction	Spr + Opx (2) + Crd + V = Krn
Late Opx rim on Bt	-

Peak metamorphism

Supplementary Table DR1: All the reactions observed in the UHT granulites of the Highland Complex, Sri Lanka. Samples with Type A and C assemblages were selected for dating.

REVISED *P-T* ESTIMATES BASED ON THERMODYNAMIC MODELING

Sajeev and Osanai (2004) estimated the peak metamorphic conditions of the studied UHT granulites to be about 1150°C at 1.2 GPa. Their calculations were based mainly on thermobarometric estimates using geothermobarometry and petrogenetic grids available at the time. They also proposed a multistage decompression path after the metamorphic peak. Building on this work and using new developments in the understanding of thermodynamic properties, Baldwin et al. (2005) suggested a new quantitative approach to interpreting the metamorphic evolution by using isochemical phase diagrams. Their estimate of the peak metamorphic temperature was similar (1110–1070°C), but their estimated pressure was lower (0.93 GPa).

By estimating the bulk chemical compositions of the peak mineral assemblage in 3107B and the retrograde assemblage in 0505E, the phase diagram, and hence *P-T* conditions, have been calculated for each. Mineral modes were determined for each micro domain using BSE imaging, then the chemical composition of the domain was calculated by summing the compositions of the individual minerals, then the results from several domains were averaged to get an effective bulk composition. The phase diagrams were computed as a function of pressure and temperature (Supplementary Figs DR1, DR2) using free energy minimization (Connolly, 2005) with end-member thermodynamic data as given by Holland and Powell (2002) and solution models as summarized in Supplementary Table DR2. Because minerals containing minor components such as CaO, Na_2O and K_2O (e.g. biotite) were not present at the peak of the retrograde decompression stage (c.f. Sajeev and Osanai, 2004), these elements were excluded from the calculation. For the peak assemblage in sample 3107B (Spr-Qtz-Grt-Opx), phase relations for the system FeO-MgO-Al_2O_3-SiO_2 were considered. For the retrograde assemblage in sample 0505E, the calculations were done for the system FeO-MgO-Al_2O_3-SiO_2-TiO_2-H_2O.

In the phase diagram for the peak mineral assemblage, the key sapphirine-quartz assemblage is stable in the low-pressure, high-temperature sector, while the assemblage orthopyroxene-sillimanite-quartz is present only in the low-pressure, low-temperature sector (Supplementary Fig. DR1). The near peak *P-T* conditions estimated using X_{Mg} [Mg/(Fe+Mg)] isopleths for garnet, sapphirine and orthopyroxene and the mineral compositions from Sajeev and Osanai (2004) yield a temperature of 1050˚C at about 0.9 GPa (Supplementary Fig. DR1). The isobaric cooling segment, which indicates consumption of sapphirine, quartz and orthopyroxene and the growth of garnet (calculated based on model proportion isopleths), is in agreement with the observed reaction microstructures. The isothermal decompression segment is also in agreement with the observed reaction microstructures which indicate orthopyroxene-sillimanite-quartz growth through the consumption of garnet. Extensive growth of sapphirine and orthopyroxene during decompression is also observed.

Supplementary table DR3. SHRIMP geochronological results for Sri Lankan UHT granulites

Grain.	Pb*	U	Th	Th	204Pb			208Pb*		208Pb*		206Pb*		207Pb*		207Pb*		Apparent ages (Ma)									
spot	ppm	ppm	ppm	U	206Pb	±	f206%	206Pb	±	232Th	±	238U	±	235U	±	206Pb	±	208/232	±	206/238	±	207/235	±	207/206	±	#Inferred	±
Grt-Spr-Opx silica-undersaturated granulite 0505E zircon																											
Cores																											
2.2	9	106	20	0.19	6.3E-05	6.4E-05	0.10	0.0578	0.0033	0.0290	0.0017	0.0931	0.0010	0.751	0.021	0.0585	0.0014	578	34	574	6	569	12	550	53	574	6
10.2	11	126	16	0.13	4.3E-05	3.3E-05	0.07	0.0400	0.0020	0.0298	0.0016	0.0935	0.0012	0.761	0.020	0.0590	0.0013	593	31	576	7	575	12	568	48	577	7
13.1	12	147	12	0.08	1.7E-04	9.1E-05	0.27	0.0228	0.0039	0.0247	0.0043	0.0906	0.0013	0.729	0.028	0.0584	0.0020	493	84	559	7	556	16	543	75	560	8
3.2	15	159	8	0.05	9.3E-06	8.1E-06	0.00	0.0186	0.0010	0.0375	0.0020	0.1007	0.0009	0.833	0.016	0.0600	0.0010	744	39	619	5	616	9	604	35	619	5
14.1	15	169	14	0.08	1.7E-04	5.6E-05	0.28	0.0203	0.0023	0.0240	0.0027	0.0957	0.0011	0.766	0.021	0.0581	0.0014	480	53	589	6	577	12	532	53	590	7
5.1	25	239	76	0.32	2.0E-05	2.0E-05	0.03	0.0969	0.0019	0.0318	0.0008	0.1044	0.0012	0.897	0.017	0.0623	0.0009	633	15	640	7	650	9	684	29	639	7
6.2	48	524	173	0.33	4.5E-05	1.8E-05	0.07	0.1000	0.0014	0.0276	0.0005	0.0914	0.0007	0.741	0.014	0.0588	0.0010	551	9	564	4	563	8	559	36	564	4
6.1	75	782	297	0.38	2.1E-05	1.2E-05	0.03	0.1150	0.0016	0.0288	0.0005	0.0952	0.0007	0.782	0.009	0.0596	0.0005	575	9	586	4	587	5	591	17	586	4
CL-dark inner overgrowths																											
4.1	26	279	109	0.39	1.2E-05	1.5E-05	0.02	0.1190	0.0028	0.0278	0.0007	0.0918	0.0007	0.747	0.011	0.0591	0.0007	554	14	566	4	567	7	569	26	566	4
1.2	42	481	162	0.34	1.8E-05	1.1E-05	0.03	0.1020	0.0021	0.0263	0.0006	0.0867	0.0007	0.697	0.009	0.0583	0.0006	524	12	536	4	537	6	542	21	536	4
5.2	65	701	281	0.40	1.9E-05	1.0E-05	0.03	0.1220	0.0012	0.0276	0.0003	0.0909	0.0005	0.733	0.010	0.0585	0.0007	551	6	561	3	559	6	550	26	561	3
Overgrowths and sector zoned																											
6.3	8	88	26	0.30	2.0E-05	2.0E-05	0.03	0.1006	0.0049	0.0296	0.0016	0.0887	0.0015	0.728	0.020	0.0596	0.0012	590	31	548	9	556	12	589	45	547	9
1.1	8	94	25	0.26	1.3E-04	6.2E-05	0.20	0.0759	0.0039	0.0248	0.0014	0.0864	0.0015	0.701	0.022	0.0589	0.0015	495	27	534	9	540	14	562	55	534	9
10.1	9	104	27	0.26	2.8E-04	9.9E-05	0.44	0.0723	0.0043	0.0248	0.0015	0.0905	0.0012	0.696	0.027	0.0558	0.0019	495	30	559	7	536	16	444	79	560	7
12.1	9	106	30	0.29	1.1E-04	7.3E-05	0.17	0.0804	0.0038	0.0254	0.0013	0.0903	0.0015	0.719	0.024	0.0577	0.0016	506	26	557	9	550	14	519	62	558	9
2.1	9	108	30	0.28	1.5E-04	1.1E-04	0.24	0.0816	0.0045	0.0257	0.0015	0.0876	0.0012	0.702	0.027	0.0581	0.0020	513	29	542	7	540	16	535	77	542	7
3.1	11	127	33	0.26	1.5E-04	6.9E-05	0.25	0.0798	0.0032	0.0270	0.0011	0.0884	0.0010	0.690	0.020	0.0566	0.0014	538	23	546	6	533	12	476	56	547	6
9.1	11	128	39	0.30	9.3E-05	4.4E-05	0.15	0.0993	0.0030	0.0292	0.0010	0.0891	0.0011	0.714	0.021	0.0581	0.0015	582	19	550	6	547	13	533	58	551	7
8.1	13	145	41	0.28	1.2E-04	6.8E-05	0.00	0.0895	0.0036	0.0288	0.0013	0.0900	0.0013	0.728	0.017	0.0587	0.0010	574	25	555	8	555	10	555	36	555	8
11.1	14	150	56	0.37	6.0E-05	5.5E-05	0.10	0.1149	0.0035	0.0277	0.0009	0.0900	0.0009	0.723	0.018	0.0583	0.0013	553	18	555	5	552	11	541	50	556	5
7.1	15	164	75	0.45	1.9E-04	6.6E-05	0.07	-	-	-	-	0.0895	0.0010	0.722	0.025	0.0585	0.0019	-	-	552	6	552	15	550	72	553	6
Grt-Spr-Opx-Qtz-Sil silica saturated granulite 3107B zircon																											
Cores																											
3.1	7	35	37	1.04	2.6E-04	2.7E-04	0.42	0.3114	0.0132	0.0505	0.0025	0.1694	0.0037	1.705	0.117	0.0730	0.0045	996	48	1009	21	1011	45	1014	131	1009	20
38.1	13	36	41	1.15	3.2E-04	1.2E-04	0.51	0.3458	0.0324	0.0900	0.0094	0.2993	0.0138	4.305	0.340	0.1043	0.0061	1741	176	1688	69	1694	67	1702	112	1702	112
27.2	18	106	56	0.53	2.7E-05	2.3E-05	0.04	0.1609	0.0033	0.0494	0.0012	0.1614	0.0019	1.625	0.053	0.0730	0.0021	975	24	964	10	980	21	1015	60	962	11
16.1	19	117	73	0.62	8.1E-05	4.2E-05	0.13	0.1897	0.0034	0.0457	0.0010	0.1497	0.0016	1.417	0.030	0.0686	0.0012	903	19	899	9	896	13	888	35	900	9
29.1	21	119	47	0.39	1.2E-05	1.3E-05	0.02	0.1160	0.0028	0.0513	0.0016	0.1745	0.0026	1.735	0.052	0.0721	0.0017	1011	30	1037	14	1022	19	989	50	1039	15
35.1	58	122	108	0.88	5.2E-06	3.6E-06	0.01	0.2586	0.0054	0.1138	0.0031	0.3888	0.0058	8.759	0.188	0.1634	0.0023	2178	56	2117	27	2313	20	2491	23	2491	23
33.1	22	141	84	0.60	1.4E-04	5.3E-05	0.22	0.1803	0.0062	0.0446	0.0017	0.1475	0.0019	1.354	0.045	0.0666	0.0019	882	32	887	11	869	20	825	62	889	11
32.1	24	154	75	0.49	1.1E-05	1.1E-05	0.02	0.1475	0.0033	0.0459	0.0013	0.1513	0.0020	1.458	0.041	0.0699	0.0016	907	24	908	11	913	17	925	48	908	12
4.1	28	163	97	0.60	5.2E-05	2.4E-05	0.08	0.1828	0.0035	0.0485	0.0012	0.1580	0.0020	1.511	0.029	0.0693	0.0009	957	22	946	11	935	12	908	27	946	11
30.1	26	168	85	0.51	1.1E-04	4.4E-05	0.17	0.1492	0.0036	0.0434	0.0013	0.1478	0.0024	1.393	0.038	0.0683	0.0014	859	25	889	14	886	16	879	42	889	14
37.1	36	189	253	1.34	5.6E-05	3.4E-05	0.09	0.3988	0.0046	0.0447	0.0009	0.1500	0.0022	1.436	0.031	0.0694	0.0010	884	18	901	12	904	13	912	29	901	12
34.1	33	190	159	0.84	4.8E-05	3.0E-05	0.08	0.2538	0.0053	0.0460	0.0013	0.1522	0.0023	1.503	0.031	0.0716	0.0009	909	24	913	13	932	13	975	26	911	13
5.1	64	212	81	0.38	1.6E-06	1.3E-06	0.00	0.1130	0.0015	0.0852	0.0013	0.2883	0.0020	4.164	0.043	0.1048	0.0007	1654	24	1633	10	1667	8	1710	13	1710	12
7.3	35	226	159	0.71	2.2E-04	6.2E-05	0.35	0.2255	0.0041	0.0441	0.0010	0.1379	0.0015	1.291	0.033	0.0679	0.0015	872	19	833	9	842	15	865	46	832	9
9.1	102	292	294	1.01	1.2E-05	1.9E-05	0.02	0.2945	0.0028	0.0843	0.0021	0.2887	0.0050	4.189	0.082	0.1052	0.0008	1636	40	1635	25	1672	16	1718	13	1718	13
17.1	105	336	81	0.24	2.5E-05	9.0E-06	0.04	0.0681	0.0030	0.0877	0.0043	0.3090	0.0065	4.532	0.152	0.1064	0.0025	1698	79	1736	32	1737	28	1738	44	1738	43
31.1	60	356	214	0.60	1.9E-05	3.7E-05	0.03	0.1786	0.0027	0.0462	0.0010	0.1558	0.0021	1.528	0.030	0.0712	0.0009	914	20	933	12	942	12	962	27	932	12
Concentric zoned																											
2.1	6	61	40	0.65	1.8E-04	8.2E-05	0.30	0.2022	0.0058	0.0290	0.0011	0.0930	0.0018	0.746	0.031	0.0582	0.0020	578	21	573	11	566	18	538	76	574	11
36.1	6	63	53	0.85	1.0E-04	9.0E-05	0.16	0.2674	0.0083	0.0282	0.0012	0.0899	0.0023	0.720	0.033	0.0581	0.0021	561	24	555	14	551	20	534	80	555	14
39.1	6	66	41	0.61	5.0E-04	1.7E-04	0.81	0.1808	0.0102	0.0271	0.0017	0.0920	0.0018	0.718	0.048	0.0566	0.0035	541	33	567	11	549	29	475	141	569	11
6.1	10	91	78	0.86	6.1E-05	7.1E-05	0.10	0.2674	0.0060	0.0293	0.0009	0.0937	0.0015	0.758	0.025	0.0587	0.0016	584	17	577	9	573	14	556	59	578	9
36.2	12	101	135	1.34	2.0E-04	1.4E-04	0.32	0.4252	0.0083	0.0289	0.0007	0.0909	0.0012	0.733	0.034	0.0585	0.0025	575	14	561	7	558	20	550	97	561	7
Sector zoned and overgrowths																											
14.1	6	43	107	2.47	6.3E-04	2.4E-04	1.01	0.7446	0.0158	0.0278	0.0009	0.0922	0.0019	0.676	0.058	0.0532	0.0043	555	17	568	11	524	36	336	193	572	11
7.1	5	44	69	1.58	2.6E-04	1.8E-04	0.42	0.5057	0.0153	0.0288	0.0011	0.0899	0.0017	0.735	0.044	0.0593	0.0033	574	21	555	10	559	26	578	125	555	10
13.1	6	51	67	1.32	6.0E-04	2.1E-04	0.00	0.4142	0.0086	0.0292	0.0008	0.0930	0.0016	0.767	0.025	0.0599	0.0016	582	16	573	9	578	15	599	58	573	9
12.1	6	54	45	0.84	2.4E-04	1.2E-04	0.38	0.2528	0.0096	0.0277	0.0012	0.0922	0.0019	0.742	0.039	0.0584	0.0027	552	24	569	11	564	23	543	104	569	11
10.1	6	56	25	0.45	2.6E-04	1.1E-04	0.41	0.1395	0.0093	0.0297	0.0021	0.0955	0.0017	0.746	0.033	0.0567	0.0022	592	41	588	10	566	19	480	88	590	10
9.2	6	62	55	0.89	7.6E-04	2.2E-04	0.00	0.2811	0.0098	0.0287	0.0012	0.0909	0.0019	0.746	0.028	0.0595	0.0017	571	24	561	11	566	16	585	63	560	11
1.1	7	78	24	0.30	5.6E-05	4.1E-05	0.09	0.0948	0.0041	0.0286	0.0014	0.0920	0.0015	0.753	0.022	0.0593	0.0014	570	27	567	9	570	13	579	50	567	9
8.1	7	83	16	0.20	5.0E-05	6.3E-05	0.00	0.0619	0.0033	0.0294	0.0017	0.0939	0.0017	0.762	0.023	0.0589	0.0013	586	33	579	10	575	13	563	49	579	10
15.1	8	86	30	0.34	2.3E-04	1.5E-04	0.00	0.1095	0.0047	0.0294	0.0014	0.0923	0.0015	0.736	0.020	0.0578	0.0012	585	27	569	9	560	12	523	45	569	9
5.2	10	116	27	0.24	2.0E-05	2.0E-05	0.03	0.0751	0.0022	0.0291	0.0010	0.0915	0.0010	0.753	0.019	0.0597	0.0013	579	19	564	6	570	11	593	48	564	6
11.1	14	136	77	0.57	1.9E-04	7.6E-05	0.31	0.1761	0.0065	0.0292	0.0012	0.0944	0.0015	0.759	0.030	0.0583	0.0020	582	23	582	9	574	17	542	76	582	9
Low Th/U outer overgrowths																											
23.1	16	189	18	0.10	7.1E-05	5.3E-05	0.11	0.0310	0.0023	0.0282	0.0021	0.0888	0.0010	0.713	0.019	0.0582	0.0013	562	42	549	6	547	11	538	50	549	6
28.1	23	266	33	0.13	5.6E-05	4.0E-05	0.09	0.0385	0.0021	0.0285	0.0016	0.0928	0.0010	0.773	0.016	0.0604	0.0010	569	31	572	6	581	9	617	37	571	6
27.1	25	292	40	0.14	1.4E-04	6.0E-05	0.06	-	-	-	-	0.0904	0.0009	0.723	0.021	0.0581	0.0015	-	-	558	5	553	13	532	59	558	5
22.1	25	303	39	0.13	9.8E-05	5.8E-05	0.16	0.0360	0.0024	0.0249	0.0017	0.0887	0.0007	0.713	0.017	0.0583	0.0012	497	33	548	4	547	10	542	46	548	4
18.1	24	306	5	0.02	8.2E-06	6.7E-06	0.01	0.0062	0.0008	0.0323	0.0043	0.0849	0.0011	0.682	0.014	0.0583	0.0009	643	84	525	6	528	9	540	34	525	6
1.2	25	311	9	0.03	6.1E-05	3.3E-05	0.10	0.0081	0.0013	0.0248	0.0039	0.0885	0.0007	0.718	0.012	0.0589	0.0008	496	78	547	4	550	7	563	30	546	4
26.1	26	316	21	0.07	2.0E-05	2.0E-05	0.03	0.0228	0.0013	0.0306	0.0018	0.0902	0.0010	0.728	0.015	0.0585	0.0010	609	35	557	6	555	9	550	36	557	6
21.1	26	321	11	0.03	5.3E-05	3.3E-05	0.02	-	-	-	-	0.0894	0.0011	0.725	0.014	0.0588	0.0008	-	-	552	6	554	8	561	30	552	6
7.2	26	347	10	0.03	3.7E-05	2.6E-05	0.06	0.0086	0.0011	0.0256	0.0032	0.0832	0.0005	0.670	0.012	0.0584	0.0009	512	62	515	3	521	7	545	36	515	3
19.1	27	347	27	0.08	3.3E-05	2.1E-05	0.10	-	-	-	-	0.0849	0.0007	0.678	0.012	0.0580	0.0009	-	-	525	4	526	7	528	34	525	4
24.1	30	349	27	0.08	1.7E-05	2.0E-05	0.01	-	-	-	-	0.0914	0.0008	0.728	0.012	0.0578	0.0007	-	-	564	5	555	7	521	28	565	5
25.1	30	359	14	0.04	3.2E-05	2.5E-05	0.05	0.0133	0.0014	0.0301	0.0032	0.0905	0.0007	0.718	0.012	0.0576	0.0008	600	63	558	4	550	7	514	32	559	4
20.1	31	377	25	0.07	7.5E-05	3.8E-05	0.03	-	-	-	-	0.0885	0.0006	0.698	0.012	0.0572	0.0008	-	-	547	4	538	7	500	33	547	4
Grt-Spr-Opx-Qtz-Sil silica saturated granulite 3107B Monazite																											
1.1	1842	130	76772	589	1.9E-04	2.2E-04	0.35	182.5	1.8	0.0275	0.0017	0.0887	0.0048	0.699	0.063	0.0571	0.0038	548	34	548	28	538	39	495	155	534	28
8.1	1634	240	66471	277	4.6E-04	1.8E-04	0.82	84.5	1.0	0.0280	0.0014	0.0918	0.0040	0.699	0.052	0.0552	0.0031	558	28	566	24	538	32	421	129	561	24
11.1	894	268	35170	131	2.0E-05	8.9E-05	0.04	41.0	0.3	0.0286	0.0013	0.0913	0.0036	0.752	0.040	0.0598	0.0018	569	26	563	21	570	23	596	66	559	21
11.2	747	344	30067	88	2.0E-05	1.1E-04	0.04	27.0	0.3	0.0276	0.0011	0.0894	0.0031	0.736	0.041	0.0597	0.0024	550	22	552	18	560	24	592	88	549	18
3.1	1157	382	46153	121	2.1E-04	1.1E-04	0.37	37.4	0.3	0.0281	0.0011	0.0908	0.0030	0.705	0.040	0.0564	0.0024	560	21	560	17	542	24	466	97	559	17
4.1	666	431	26215	61	2.0E-05	5.0E-05	0.04	18.8	0.1	0.0277	0.0007	0.0898	0.0019	0.754	0.024	0.0609	0.0013	553	14	554	12	570	14	636	45	551	12
6.2	1718	466	69930	150	5.0E-04	1.4E-04	0.89	45.3	0.5	0.0277	0.0009	0.0918	0.0025	0.679	0.040	0.0536	0.0027	552	18	566	15	526	25	356	115	566	15
6.4	1092	486	44475	92	8.2E-05	1.7E-04	0.15	28.1	0.3	0.0273	0.0007	0.0889	0.0020	0.697	0.041	0.0569	0.0029	544	15	549	12	537	25	486	117	548	12
9.1	956	2001	32131	16	2.0E-05	1.5E-05	0.04	5.03	0.02	0.0284	0.0003	0.0905	0.0009	0.734	0.011	0.0588	0.0005	566	7	559	5	559	6	559	20	558	5
3.2	715	2030	22946	11	2.0E-05	1.8E-05	0.04	3.61	0.02	0.0278	0.0005	0.0872	0.0012	0.706	0.013	0.0588	0.0007	555	9	539	7	542	8	558	24	538	7
6.3	1666	2880	62580	22	1.1E-04	3.0E-05	0.19	6.67	0.05	0.0265	0.0004	0.0864	0.0010	0.683	0.013	0.0573	0.0008	529	8	534	6	528	8	503	30	534	6
6.1	478	3902	4663	1.2	2.0E-05	2.2E-06	0.04	0.36	0.00	0.0303	0.0004	0.1001	0.0008	0.828	0.009	0.0600	0.0003	603	7	615	5	613	5	603	12	616	5
1.2	1329	5054	37107	7.3	3.8E-05	1.5E-05	0.07	2.35	0.01	0.0285	0.0005	0.0891	0.0014	0.737	0.013	0.0599	0.0004	568	10	550	8	560	8	601	15	549	8
6.5	688	5812	6429	1.1	2.0E-05	1.9E-06	0.04	0.35	0.00	0.0308	0.0004	0.0975	0.0009	0.805	0.009	0.0599	0.0003	613	8	600	5	600	5	599	12	600	5
6.6	2650	7550	86979	12	2.7E-05	1.3E-05	0.05	3.54	0.02	0.0271	0.0003	0.0881	0.0008	0.728	0.009	0.0600	0.0005	540	6	544	5	556	5	603	17	543	5

* Radiogenic. Corrected for common Pb using 204Pb or 208Pb, and a Pb isotopic composition based on the Pb evolution model of Cumming and Richards (1975).
f206%. Percentage of total 206Pb that is common 206Pb.
Best estimate of the spot age. 206/238 age corrected for common Pb using 207Pb (age < 1.5 Ga) or 207/206 age corrected for common Pb using 204Pb (age > 1.5 Ga).

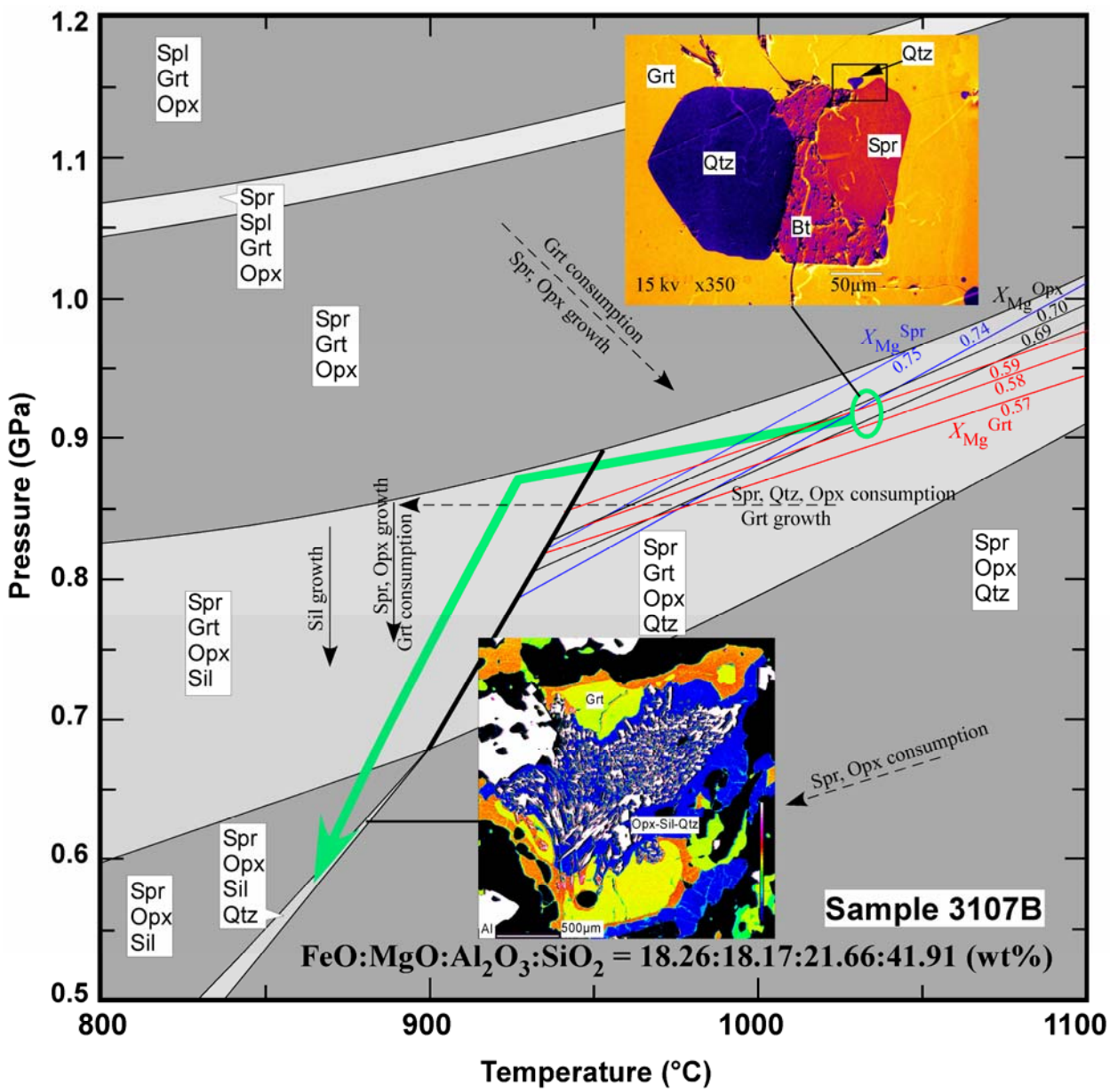

Supplementary Figure DR1: Phase diagram calculated for the peak UHT mineral assemblage from silica saturated sample 3107B of the Highland Complex, Sri Lanka. The top inset is a false-color BSE image of the Spr-Qtz association within a garnet core (modified after Sajeev and Osanai, 2004). The bottom inset is an X-ray map of Al in the retrograde Opx-Sil-Qtz assemblage formed at the expense of garnet.

Sample 0505E consists mainly of retrograde symplectite microstructures indicating the growth of sapphirine-orthopyroxene-cordierite at the expense of garnet. Melt is stable only on

the high temperature side of the phase diagram. No evidence for the former presence of melt has been found either in the studied sample or in the field. An isothermal decompression path can be derived from the compositional and model proportion isopleths. This is consistent with the symplectite structures present in the sample.

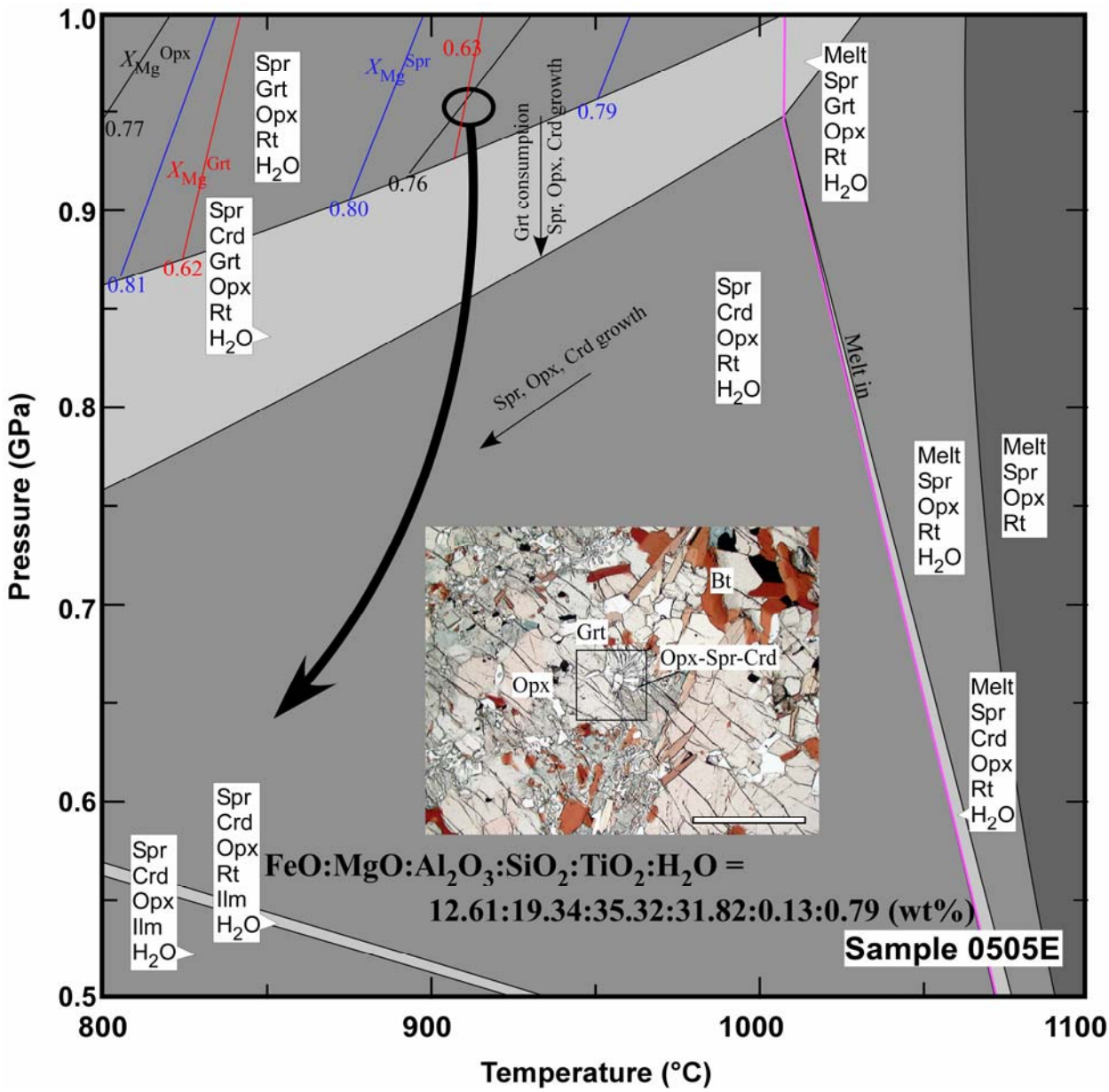

Supplementary Figure DR2: Phase diagram calculated for the retrograde symplectite assemblage from silica undersaturated sample 0505E of the Highland Complex, Sri Lanka. Inset shows the Opx-Spr-Crd symplectite after garnet (after Sajeev and Osanai, 2004). Scale bar 1 mm.

The cumulative *P-T* path indicates a cooling from UHT conditions followed by isothermal decompression. The identified *P-T* segments are similar to those proposed by Sajeev and Osanai (2004).

Supplementary Table DR2. Solution notation, formulae and model sources for phase diagram calculations.

Symbol	Solution	Formula	Source
Opx	orthopyroxene	$[Mg_xFe_{1-x}]_{4-2y}Al_{4(1-y)}Si_4O_{12}$	1
Grt	garnet	$Fe_{3x}Ca_{3y}Mg_{3(1-x+y+z/3)}Al_{2-2z}Si_{3+z}O_{12}$, $x+y\leq1$	2
Melt	melt	Na-Mg-Al-Si-K-Ca-Fe hydrous silicate melt	3, 4
Spr	sapphirine	$[Mg_xFe_{1-x}]4-y/2Al_9-ySi_2-y/2O_{20}$	5

Unless otherwise noted, the compositional variables *x*, *y*, and *z* may vary between zero and unity and are determined as a function of the computational variables by free-energy minimization.
Sources: 1 –Holland and Powell, 1996; 2 – Holland and Powell, 1998; 3 – Holland and Powell, 2001; 4-White et al. (2001); 5-Kelsey et al. (2004)

SHRIMP GEOCHRONOLOGY ANALYTICAL METHODS

About 300 g of each rock sample were crushed to <250 µm and the high-density minerals extracted using clean density and magnetic separation procedures. Final purification was by hand picking. Zircon and monazite were mounted separately in epoxy resin with grains of reference material; zircon FC1 ($^{206}Pb^*/^{238}U$ = 0.1859) and SL13 (238 ppm U), and monazite Thompson Mine WB.T.329 ($^{206}Pb^*/^{238}U$ = 0.3152, 2100 ppm U). Mounts were polished to expose the crystal interiors, photographed in transmitted and reflected light, then washed and Au coated before analysis. Prior to analysis, the zircons also were imaged by cathodoluminescence (CL) using an Hitachi S-2250N SEM to document their internal textures. Monazite textures were imaged by backscattered electron (BSE) using a Cambridge Instruments Stereoscan 360.

U-Th-Pb were analysed on the RSES SHRIMP II ion microprobe using procedures similar to those described by Williams et al. (1996). A primary ion beam of ~3 nA, 10 kV O_2^- was focused to a probe ~25 µm diameter and the sputtered secondary ions extracted at 10 kV, mass analysed at a resolution of ~5000, and the Ce, Zr, Pb, U and Th species of interest measured on a single electron multiplier by cyclic stepping of the analyser magnet field. Moderate energy filtering was used for the monazite analyses to reduce a molecular isobaric interference at mass 204. Isotopic

compositions were measured directly, without correction for mass fractionation. Common Pb was corrected using ^{204}Pb or ^{208}Pb, assuming a common Pb isotopic composition based on the Pb evolution model of Cumming and Richards (1975). Corrections for Pb-U fractionation utilised a power law relationship between Pb^+/U^+ and UO^+/U^+ (Claoué-Long et al., 1995). The correction factor for Th-U fractionation in monazite was calculated directly from a $^{208}Pb/^{206}Pb$-ThO/UO isochron as outlined by Williams et al. (1996). Analytical uncertainties listed in the table and plotted in the figures are one standard error precision estimates. Ages were calculated using the constants recommended by the IUGS Subcommission on Geochronology (Steiger and Jäger, 1977). Uncertainties in the ages cited in the text are 95% confidence limits, namely $t\sigma$, where t is 'Student's t', and include the uncertainties in the standard calibrations (zircon 0.2–0.5%, monazite 0.4%). Detailed analytical results are in Supplementary table 2.

Th/U

The significance of the range in Th/U in the different generations of zircon growth is discussed in the main text.

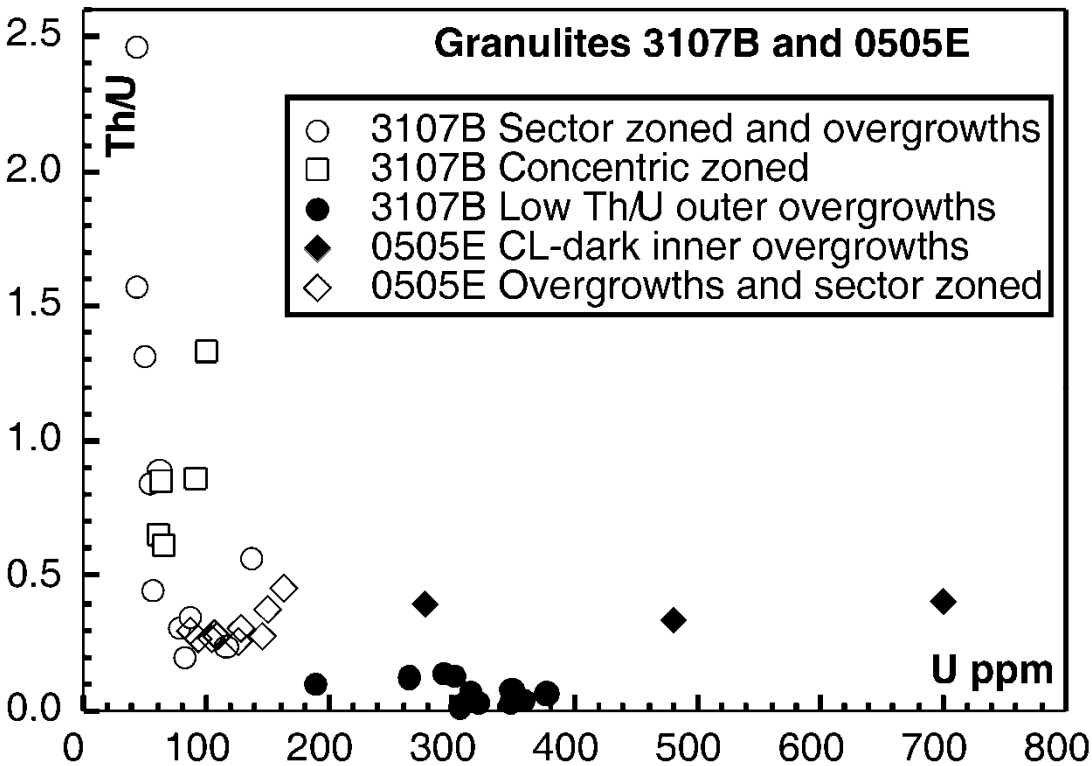

Supplementary Figure DR3: Contrasting U contents and Th/U in different generations of metamorphic zircon from samples of Sri Lankan Qtz-bearing and Qtz-free UHT granulites.

REFERENCES CITED

Baldwin, J.A., Powell, R., Brown, M., Moraes, R., and Fuck, R.A., 2005, Modelling of mineral equilibria in ultrahigh-temperature metamorphic rocks from the anápolis-Itauçu Complex, central Brazil. Journal of Metamorphic Geology, v. 23, p. 511-531.

Claoué-Long, J.C., Compston, W., Roberts, J., and Fanning, C.M., 1995, Two Carboniferous ages: A comparison of SHRIMP zircon dating with conventional zircon ages and 40Ar/39Ar analysis, *in* Berggren, W.A., Kent, D.V., Aubrey, M-P., and Hardenbol, J., eds., Geochronology, Time Scales and Global Stratigraphic Correlation, Society for Sedimentary Geology, Special Publication 4, p. 3–21.

Connolly, J.A.D., 2005, Computation of phase equilibria by linear programming: A tool for geodynamic modeling and its application to subduction zone decarbonation. Earth and Planetary Science Letters, v. 236, p. 524–541.

Cumming, G.L., and Richards, G.R., 1975, Ore lead isotope ratios in a continuously changing earth. Earth and Planetary Science Letters, v. 28, p. 155–171.

Holland, T.J.B., and Powell, R., 1996, Thermodynamics of order-disorder in minerals.2. Symmetric formalism applied to solid solutions. American Mineralogist, v. 81, p. 1425-1437.

Holland, T.J.B., and Powell, R., 1998, An internally consistent thermodynamic data set for phases of petrological interest. Journal of Metamorphic Geology, v. 16, p. 309-344.

Holland, T.J.B., and Powell, R., 2001, Calculation of phase relations involving haplogranitic melts using an internally consistent thermodynamic dataset. Journal of Petrology, v. 42, p. 673-683.

Kelsey, D.E., White, R.W., Holland, T.J.B., and Powell R., 2004, Calculated phase equilibria in K2O-FeO-MgO-Al_2O_3-SiO_2-H_2O for sapphirine-quartz-bearing mineral assemblages. Journal of Metamorphic Geology, v. 22, p. 559–578.

Sajeev, K., and Osanai, Y., 2004, Ultrahigh-temperature metamorphism (1150° C, 12kbar) and multistage Evolution of Mg-, Al-rich granulites from the Central Highland Complex Sri Lanka. Journal of Petrology, v. 45, p. 1821–1844.

Steiger, R. H., and Jäger, E., 1977, Subcommission on geochronology: convention on the use of decay constants in geo- and cosmochronology. Earth and Planetary Science Letters, v. 36, p. 359–362.

White, R.W., Powell R., and Holland T.J.B., 2001, Calculation of partial melting equilibria in the system Na2O-CaO-K_2O-FeO-MgO-Al_2O_3-SiO_2-H_2O (NCKFMASH). Journal of Metamorphic Geology, v. 19, p. 139-153.

Williams, I.S., Buick, I.S., and Cartwright, I., 1996, An extended episode of early Mesoproterozoic metamorphic fluid flow in the Reynolds Range, central Australia. Journal of Metamorphic Geology, v. 14, p. 29–47.